# Exergy analysis and thermo-economic optimization of a district heating network with solar- photovoltaic and heat pumps

Getnet Tadesse Ayele, Mohamed Mabrouk, Pierrick Haurant, Björn Laumert, Bruno Lacarrière, Massimo Santarelli

# Exergy analysis and thermo-economic optimization of a district heating network with solar-photovoltaic and heat pumps

Getnet Tadesse Ayele[1,2,*], Mohamed Tahar Mabrouk[1], Pierrick Haurant[1], Björn Laumert[2], Bruno Lacarrière[1], Massimo Santarelli[3]

**Abstract**

Electrification of district heating networks, especially using heat pumps, is widely recommended in literature. Installing heat pumps affects both electricity and heating networks. Due to lack of suitable modelling tools, size optimization of heat pumps in the heating network with the full consideration of the electric distribution network is not well addressed in literature. This paper presents an optimization of a district heating network consisting of solar photovoltaic and heat pumps with the consideration of the detail parameters of heating and electric distribution networks. An extended energy hub approach is used to model the energy system. Exergy and energy analyses are applied to identify and isolate lossy branches in a meshed heating network. Both methods resulted into the same reduced topology. Particle swarm optimization is then applied on the reduced topology in order to find out the most economical temperature profiles and size of distributed heat pumps. The thermo-economic results are found to be highly influenced by the heat demand distribution, the power loss in both electric and heat distribution network, the cost of generation, the temperature limits and the coupling effect of the heat pumps.

***Key Words***: *electrification of district heating network, energy hub, exergy, multi-carrier energy systems, particle swarm optimization, thermo-economic optimization*

## 1. Introduction

District heating network (DHN) transports heat using hot water as a media. The temperature levels and the mass flows determine the amount of heat injected into the network from the sources, the distribution loss and the amount of heat consumed at the consumers [1]. For a given heat demand, a higher source temperature results in a higher temperature difference with the surrounding environment. It also means a lower mass flow rate and lower pumping energy requirement [2]. However, the water will have higher residence time in the pipe. This causes a higher percentage of the heat flowing in the pipe to be dissipated. From exergy point of view, a higher temperature means a higher quality of heat [3]. On the other hand, district heating networks are designed mainly to harness energy from cheap low-grade heat sources (characterized by lower temperature) and distribute it to the end users [1]. Hence, operating these networks at lower temperature makes them more effective from the source temperature level point of view. As a lower supply temperature means a higher mass flow rate and, as a result, a lower residence time in the pipe, it decreases the heat that could be lost in the network. However, a higher mass flow rate means a higher pumping energy to circulate the water throughout the pipe network. The circulating pump uses electricity which is regarded as a very high quality, also referred as a pure exergy [3,4]. The trade-off between temperature levels, distribution loss and the pumping energy, therefore, needs optimization.

The low-grade heat sources may not be enough to supply all the heat demand. In that case, heat pumps and gas fired combined heat and power (CHP) plants can also be used as a source of heat which are relatively more expensive. The optimal location of these plants, their size and operating temperatures should be included in the optimization in order to have a cost-effective operation of the DHN.

[1] IMT Atlantique, Department of Energy Systems and Environment, GEPEA, F-44307 Nantes

[2] Department of Energy Technology, KTH Royal Institute of Technology, 100 44 Stockholm, Sweden

[3] Dipartimento di Energetica, Politecnico di Torino, Corso Duca degli Abruzzi 24, 10129 Torino, Italy

* Corresponding author (email address: gtayele@kth.se (G.T. Ayele))

Exergy analysis, which considers both quantity and quality of energy, can be used to optimize thermal systems [4]. DHNs are one of such systems where exergy analysis can be applied to identify lossy branches and nodes in a meshed network topology. Many literatures focused on the exergy analysis of the heat source power plants rather than the heat distribution network. Yao et al. [5], for example, studied the thermo-economic optimization of combined heating, cooling and power plants. Wang et al. [6] followed a similar approach to study a combined cooling, heating and power plant assisted with solar system. Exergy analysis of heat pumps is discussed by Dincer and Rosen [4] and Bilgen and Takahashi [7].

On the other hand, there are only limited exergy related researches conducted on the heat distribution networks. Vincio et al. [8] used exergy analysis to optimize emissions from a district heating system. Only emissions from power plants are considered in their study. Terehovics et al. [9] also applied exergy factor to identify the most influential component of a district heating network. Li and Svendsen [10] used both energy and exergy analysis to study the performance of low temperature district heating networks in comparison to medium and high temperature district heating networks. They found that low temperature district heating networks have lower exergy and energy losses. Coss et al. [11] used exergy cost analysis to determine the unit exergy cost of each node in a radial heat distribution network. Transient analysis based on graph-based representation are considered in the determination of temperature and mass flows in the network. Only supply pipe networks are considered in their analysis. The exergy loss on the return network, the exergy requirement due to circulation pumps are not dealt in detail.

Once the critical and lossy components are identified using exergy/energy analysis, it is usually followed by optimization of operational parameters. Both mathematical and heuristic/metaheuristic approaches of optimizing energy systems are reported in literature. The management of future energy system, with respect to smart grids and distributed generations, is obvious to become more complex due to the interdependency between different energy carriers. Analysing and optimizing such systems mathematically will be cumbersome, if not impossible. Thanks to the computational power of computers, heuristic optimization techniques are getting wider acceptance as they are more suitable to handle highly nonlinear objective functions and constraints than the conventional deterministic approaches.

The level of optimization can be categorized into two: those at feasibility level and those at operational level. For example, HOMER [12] and RETScreen [13] can be used for size optimization of hybrid energy systems at feasibility level. The details of network topology and operational parameters are not considered in such tools. PowerWorld [14], on the other hand, considers operational network parameters to solve the economical dispatch and optimal power flow of electrical network. Some of the heuristic algorithms that are used in the energy field include: Genetic Algorithm (GA) [15,16], Teaching Learning Based Algorithms (TLBA) [17,18], Honey Bee Mating Algorithms (HBMA) [19], Mixed Integer Linear Programming (MILP) [15,20,21], and Particle Swarm Optimizations(PSO) [22–25].

Two main gaps are identified that are not well addressed in the literatures discussed above:

1. The temperature and pressure variations across the pipes of DHN, both on the supply and return sides, are not considered well in the exergy analysis.
2. The details of the electricity network parameters and the associated power losses are not taken in to account in thermos-economic optimization of DHN consisting of coupling devices such as HPs.

This paper tries to fill these gaps by combining a previously developed MCES model, called an extended energy hub modelling approach, with a heuristic optimization, such as particle swarm optimization (PSO) algorithm. Though the extended energy hub modelling approach is general and flexible enough to model varieties of coupling technologies with different energy carriers [26], the scope of this paper is limited to only electricity and heating distribution networks

consisting of solar PV and HPs. The model is used to formulate and solve the steady state load flow problems for both networks simultaneously. The details of network parameters that are determined by the load flow, such as temperature, mass flow rate and hydraulic heads on both supply and return pipe networks of the DHN, are explicitly included in the calculations of exergy efficiency for each branch and node in the DHN. Once lossy branches are isolated, thermos-economic optimization is conducted on the reduced network topology using PSO technique. Temperature levels, cost of pumping energy, cost of electricity, cost of heat, capacity limits in both electricity and heating networks and sizes of HPs are considered in the optimization. More details about the methodology followed in this paper are discussed in Section 2. Section 3 describes the parameters of a network topology which is taken as a case study. Section 4 presents the results and discussions while Section 5 concludes the main findings of the paper.

## 2. Methodology

### *2.1. System model*

An extended energy hub approach, the details of which can be found in [26], is used in this paper to model the interaction between different energy carriers including different energy conversion technologies. Figure 1 shows the three parts in the extended representation of a general MCES: *the energy hub, the point of interconnection*[4] *and the energy network*. Local demands, local generations and coupling devices are altogether represented by the energy hub while the point of interconnection acts as an interface btween the energy hub and the remaining part of the the network. Coupled electricity and heating networks are considered in this paper. The main focus is, however, on the heating network part. The electrical distribution network is considered only for the purpose of delivering the electricity required by the DHN. No electrical load is considered at each hub. By doing so, the electricity lost in the network can be computed and taken into account in the optimization (see section 2.3).

For each hub $k$, the per unit active ($P_{el}$) and reactive ($Q_{el}$) power injections, which are given by (1a) and (1b), defines the electrical sub-model [26]. These equations are used to determine the electrical network parameters such as voltage magnitude, voltage angle, active and reactive power flows and losses in the network.

$$P_{el(k)} = \sum_{j=1}^{N} |V_k|\,|V_j|\left(G_{kj}cos\theta_{kj} + B_{kj}sin\theta_{kj}\right) \quad (1a)$$

$$Q_{el(k)} = \sum_{j=1}^{N} |V_k|\,|V_j|\left(G_{kj}sin\theta_{kj} - B_{kj}cos\theta_{kj}\right) \quad (1b)$$

where $\theta_{kj}$ is the voltage angle difference between bus $k$ and bus $j$; $G_{ij} + jB_{ij} = Y_{ij}$ is an element of the network admittance matrix, $N$ is number of buses and $|V_k|$ is voltage magnitude at bus $k$.

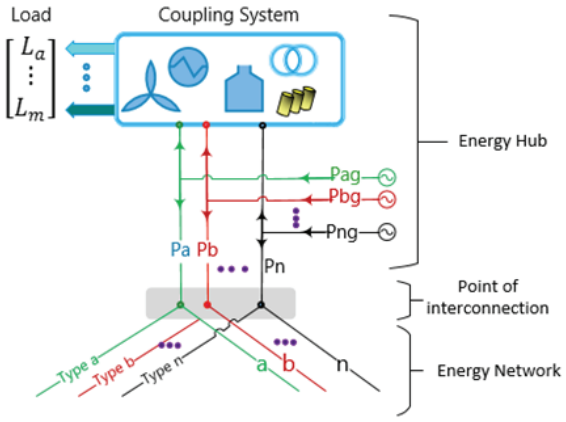


*Fig. 1. An extended energy hub representation in a general MCES* [26]

[4] The point of interconnection refers to a bus in electricity network and a node in a heating network [26].

On the other hand, the steady state thermo-hydraulic model of a district heating network is defined by (2) – (6) [26]. These equations are used to determine the heating network parameters, such as temperature, mass flow rate, heat power flows and hydraulic heads. The heat power injection ($P_h$) into the network from hub *k* is given by (2).

$$P_{h(k)} = C_p \dot{m}_k (T_{sk} - T_{rk}) \quad (2)$$

where $\dot{m}_k$ is the nodal mass flow rate flowing from hub *k* into the supply pipe network of the DHN; $T_{sk}$ and $T_{rk}$ are supply and return temperatures at hub *k* respectively and $C_p$ is specific heat capacity of water.

The nodal mass flows ($\dot{m}_k$) are subjected to the continuity of flow equations given by (3) which relates nodal flows with the pipe flows. The pipe flows are further related to the hydraulic heads using pressure drop equations, as defined in (4).

$$\sum_k(\text{all mass flows into the node}) = \sum_k(\text{all mass flows out of the node}) \quad (3)$$

$$H_j - H_i = K_{ij} \dot{m}_{ji} |\dot{m}_{ji}| \quad (4)$$

where $H_i$ and $H_j$ are hydraulic heads at nodes *i* and *j*; $\dot{m}_{ji}$ is pipe mass flow from node *j* to node *i* and $K_{ij}$ is the corresponding pressure resistance coefficient.

Equation (5) describes the energy balance of mixing water at a given node while (6) represent the temperature drop across a pipe.

$$\sum(\mathrm{T_{j-in}} \dot{\mathrm{m}}_{\mathrm{j-in}}) = \mathrm{T_{j-out}} \sum(\dot{\mathrm{m}}_{\mathrm{j-out}}) \quad (5)$$

$$T_{w\_end} - T_o = (T_{w\_start} - T_o) e^{-\left(\frac{2\pi ZLU}{C_p \dot{m}}\right)} \quad (6a)$$

$$U = \left(\frac{R_4}{R_1 h_w} + \frac{R_4}{k_2} ln\left|\frac{R_2}{R_1}\right| + \frac{R_4}{k_3} ln\left|\frac{R_3}{R_2}\right| + \frac{R_4}{k_4} ln\left|\frac{R_4}{R_3}\right|\right)^{-1} \quad (6b)$$

where $(\dot{m}_{j-in}, T_{j-in})$ terms are the incoming mass flow rates and water temperatures at a given node *j* while $(\dot{m}_{j-out}, T_{j-out})$ terms are the outgoing mass flow rates and water temperature at the same node *j* respectively; $T_{w\_end}$ and $T_{w\_start}$ are outlet and inlet water temperatures, respectively. $T_o$ is the soil temperature at the surface of the pipe; *U* is the overall heat transfer coefficient; $R_1, R_2, R_3$and $R_4$ are the inner radius of carrier pipe, outer radius of the carrier pipe, outer radius of an insulation layer and outer radius of an outer jacket, respectively; $h_w, k_2, k_3$ and $k_4$ represent the convective coefficient of water, thermal conductivity of carrier pipe, thermal conductivity of the insulating material and thermal conductivity of the outer jacket.

In addition to the above equations, which govern the network part of the energy system, there are additional equations which govern the conversion relationships between different energy carriers at each hub. These equations, as shown in (7), relates the demands, generations, injections into the network and conversion between different energy carriers at a given hub [26,27].

$$\begin{bmatrix} L_{Pel(k)} \\ L_{Qel(k)} \\ L_{h(k)} \end{bmatrix} = \begin{bmatrix} C_{k-ep(ep)} & C_{k-ep(eq)} & C_{k-ep(h)} \\ C_{k-eq(ep)} & C_{k-eq(eq)} & C_{k-eq(h)} \\ C_{k-h(ep)} & C_{k-h(eq)} & C_{k-h(h)} \end{bmatrix} \begin{bmatrix} P_{elg(k)} - P_{el(k)} \\ Q_{elg(k)} - Q_{el(k)} \\ P_{hg(k)} - P_{h(k)} \end{bmatrix} \quad (7)$$

where $L_{Pel(k)}$, $L_{Qel(k)}$ and $L_{\mathrm{h}(k)}$ are the active electricity, reactive electricity and heat demands at hub *k*; $C_{k-\delta(\gamma)}$ represent a coupling coefficient at hub *k* relating generation type $\gamma$ with load type $\delta$; *ep, eq and h* indicate active electric, reactive electric and heat carriers, respectively; $P_{elg(k)}$, $Q_{elg(k)}$ and $P_{hg(k)}$ are active electricity, reactive electricity and heat power locally generated at hub *k*.

### *2.2. Exergy analysis*

Equations (1) - (7) are solved using Newton-Raphson iterative methods to determine the operating conditions of the DHN and electric distribution network. The load flow solution is then used to calculate exergy flows in the DHN. The exergy

streams involved in the DHN are the water flows at different temperature and pressure. These physical exergies are computed using (8) [3,4].

$$B_{ph} = \dot{m}\left\{C_p\left(T - T_o - T_o ln\frac{T}{T_o}\right) + \frac{P-P_o}{\rho}\right\} \quad (8)$$

where $B_{ph}$ is the physical exergy of a mass flow $\dot{m}$ at temperature $T$ and pressure $P$ with respect to the restricted dead state reference of temperature, $T_o$ and pressure, $P_o$; $\rho$ is density of water; In this paper, a temperature of 283.15K, which is equal to the presumed soil temperature at the surface of the pipe, and a pressure of $10^5$ Pa, which is equivalent to atmospheric pressure, are taken as restricted dead state references.

The electricity consumption by the circulation pump for each pipe is considered as a pure exergy. For a given branch, the same mass flows on both supply and return pipes which implies that the same amount of electricity is consumed by each of the circulation pumps on the return and supply pipes. Hence, the electricity consumed by the branch, $W_e$, to compensate the pressure drop on both supply and return sides can be computed using (9).

$$W_e = 2\left(\frac{g*dH_{ij}*|\dot{m}_{ij}|}{\eta}\right) \quad (9)$$

where $g$ is gravitational acceleration, $dH_{ij}$ is the pressure head difference between nodes *i* and *j*; $|\dot{m}_{ij}|$ is magnitude of the mass flow in the pipe and $\eta$ is efficiency of the circulation pump (it is assumed to be 80%).

### *2.3. Particle Swarm Optimization (PSO)*

First developed by Kennedy and Eberhart [28] in 1995, PSO is an optimization algorithm which tries to find the global best value in analogy to the way a flock of birds scatter and regroup. The whole group is referred to as a swarm and its individual members are called particles. If there are *M* variables of optimization, then each particle in the swarm defines a point in *M*-dimensional space, usually referred to as position of the particle. In each iteration, all the particles try to adjust their position by taking their own past experience and the social knowledge into account. Randomness is also included in the algorithm to minimize the possibility of being trapped by a local optima. The position of particle *i* with *M* number of optimization variables is defined as shown in (10a).

$$x_i = (x_{i1}, x_{i2}, \dots, x_{iM}) \quad (10a)$$

The new direction and speed of the particle ($v_{i-new}$) is updated using (10b). Using the new velocity of the particle, the new position of the particle ($x_{i-new}$) is calculated as shown in (10c).

$$v_{i-new} = \omega v_{io} + c_1 r_1(x_{i-best} - x_i) + c_2 r_2(x_{g-best} - x_i) \quad (10b)$$

$$x_{i-new} = x_i + v_{i-new} \quad (10c)$$

where $\omega$ is the inertia/damping factor; $v_{io}$ is the current velocity of particle *i*; $c_1$ is a self-accelerating (exploration) factor; $c_2$ is a global accelerating (exploiting) factor; $x_i$ is the current position of particle *i*; $x_{i-best}$ is the best position of the particle in the past; $x_{g-best}$ is the global best position achieved by the swarm in the past; $r_1$ and $r_2$ are random numbers between 0 and 1.

Though there is no strictly binding rule in selecting the values of $\omega$, $c_1$ and $c_2$, Aote et al. [22] argues that better results are found using a step by step variation of parameters in the following order: $c_1$decreasing from 2.5 to 0.5 and $c_2$ increasing from 0.5 to 2.5. The same strategy is employed in this paper and $\omega$ is made to vary from 0.9 to 0.4.

The objective function of the optimization, as given in (11), is minimization of the operating cost of the district heating network. There are both equality and inequality constraints that should not be violated while achieving the objective

function. All the equations (1) – (7) are taken as equality constraints while equations (12a) - (12e) are the main inequality constraints. Equation (12a) defines the bus voltage limits; equation (12b) defines the maximum transmission line ampacity either in the form of root mean square (rms) current or kW power [29]; equation (12c) defines the maximum allowed mass flow in each pipe [30]; equation (12d) sets the limit on the supply temperature of heat source hubs and equation (12e) defines the allowed return temperature from heat consuming hubs. The temperature limits depend on the characteristics of heat sources, the temperature levels required at the secondary side of heat consumers and the regulations of the municipality, such as Legeionellosis issues [1]. Additional constraints on the sizes of power plants and heat pumps are discussed in Section 3.

$$min\{C_{Phg} + C_{Pelg} + C_{Ph-imported} + C_{Pel-imported} + C_{We}\} \quad (11)$$

where $C_{Phg}$, $C_{Pelg}$, $C_{Ph\text{-}imported}$, and $C_{Pel\text{-}imported}$ are costs of the generated heat, generated electricity, imported heat and imported electricity, respectively while $C_{We}$ is the cost of electricity used for circulation pumps.

$$0.95 \leq \left|V_{k(perunit)}\right| \leq 1.05 \quad (12a)$$

$$0 \leq \left|I_{ij(rms)}\right| \leq 185A, \textit{ or equivalently, } 0 \leq \left|P_{el(loss)ij}\right| \leq 6.3kW \quad (12b)$$

$$0 \leq \left|\dot{m}_{ij}\right| \leq 1.4\ kg/s \quad (12c)$$

$$65℃ \leq T_{s(k)} \leq 95℃, \textit{for } \dot{m}_k \gg 0 \quad (12d)$$

$$30℃ \leq T_{r(k)} \leq 55℃, \textit{for } \dot{m}_k \ll 0 \quad (12e)$$

## 3. Case study

A hypothetical district heating network with six nodes and two loops, shown in Fig 2, is considered as a case study. The solid lines with arrow represent the supply pipe network while the dotted lines with arrow represent the return pipe network of the DHN. The black solid lines without arrow represent the electric distribution network. Each of the grey circles represents node/bus at which the corresponding hub interacts with the network. Each hexagon represents an energy hub consisting of energy conversion devices, demands and local production of heat and electricity. The details of the pipe and insulation parameters together with the resistance and reactance of the electrical transmission lines are described Table A-1, Appendix A.

Hub1 is considered as a slack hub from which the deficit in heat and electric power balance is compensated from the neighbourhood networks. It also acts as a point of export to the neighbourhood should the district network have excess production than what is required. Hub 2, 4 and 6 are connected with heat consumers. Hub5 is assumed to have a solar PV generation of 40kW. HPs are considered as a means of coupling between the electricity and heating networks.

The analysis is conducted in four different scenarios. The first two scenarios deal with topology reduction with fixed generation and temperature profiles while the last two scenarios deal with thermo-economic optimization on the reduced topology. The loading and HP sizes for each scenario are summarised in Table 1. In Scenario I, a 100kW heat demand is assumed at each of the Hubs 2, 4 and 6. Hubs 3 and 5 are selected as sources of heat so that there will be transport of heat throughout the network to meet the demands located at Hubs 2, 4 and 6. This will help to identify the lossiest branch from those which are part of the two loops. Accordingly, a HP of 40kWe electrical rating running at full load with a coefficient of performance (COP) of 4 is assumed to be connected at each of Hub 3 and Hub 5. All sources' temperatures of are assumed to be at 85°C while all the return temperatures from the consumers are set at 35°C. The steady state load flow is then performed to determine the operational state of the network.

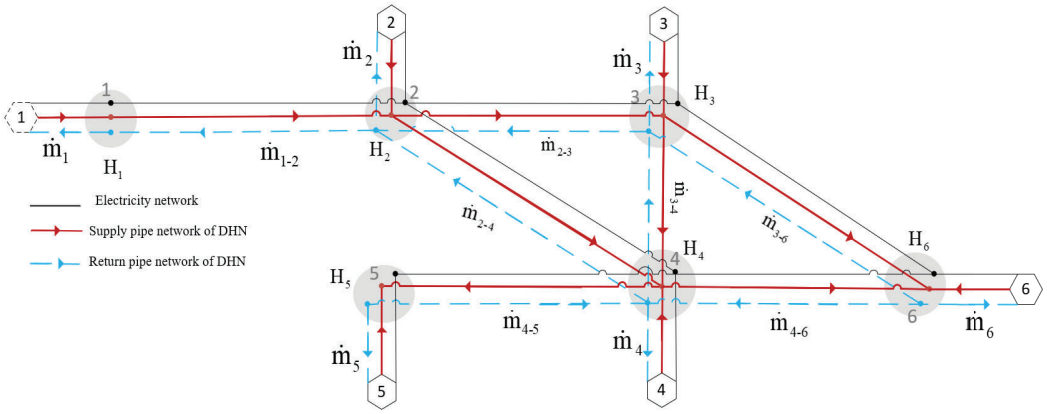


*Fig. 2 A small hypothetical heating network*

Table 1: Description of scenarios

| Hub | Scenario I | Scenario II | Scenario III | Scenario IV |
|---|---|---|---|---|
| 1 | Slack hub | Slack hub | Slack hub | Slack hub |
| 2 | 100kW of heat load | 100kW of heat load | Heat load, HP (0 – 25kWe) | Heat load, HP(0 – 25kWe) |
| 3 | 40kWe HP running at full load | 40kWe HP running at full load | HP (0 – 25kWe) | HP (0 – 25kWe) |
| 4 | 100kW of heat load | 100kW of heat load | 100kW of heat load | 60kW of heat load, HP (0 – 25kWe) |
| 5 | 40kWe HP running at full load | 40kWe HP running at full load | HP (0 – 25kWe) | HP (0 – 25kWe) |
| 6 | 100kW of heat load | 100kW of heat load, | 100kW of heat load, HP (0 – 25kWe) | 140kW of heat load, HP (0 – 25kWe) |

Scenario II is the same as Scenario I except that the lossy branches are isolated in the former case. Scenario III deals with cost and temperature optimization after the lossy branches are isolated. PSO is used with 150 a population size of and 200 maximum iteration. In addition to the constraints listed in (12), a continuous range of 0 – 25kWe HPs at COP of 4.0 are considered as variables of optimization. A price of 0.20€/kWh of electricity and 0.10 €/kWh of heat are assumed at Hub 1. The operating cost of the solar PV is assumed to be zero. Scenario IV is the same as Scenario III except that the heat demand at Hub 4 is reduced by 40kW while the demand at Hub 6 is increased by 40kW.

## 4. Results and discussions

### *4.1. Identifying lossy branches (Scenarios I & II)*

The hub level load flow results of Scenario I are presented in Table 2 while the branch parameters of the DHN are summarised in Table 3. The total amount of heat demand is 300kW. To meet this demand, 320kW of heat is generated from the two HPs using 80kW of electricity. Although the generated heat from the two HPs was 20kW more than the total heat demand, it was not enough to compensate the losses in the network. Hence, additional 99.75kW of heat is imported from the neighbourhood. The total heat loss in this network is about 119.75kW giving a DHN energy efficiency of 71.47%. The electricity lost in the distribution network is 0.0231kW which accounts 0.029% of the total electricity demand of HPs. Table 3 also shows the amount of heat transported by each branch and their corresponding efficiencies. It is clear that branch 2-4 is dissipating all the incoming heat from the two nodes and shall be isolated. This is due to the lowest mass flow rate in the pipe which resulted into a temperature drop from 77.17℃ to 13.02℃ on the supply side and from 35℃ to 11.12℃ on the return side of the DHN (see Table 3). The next lossy branches, according to their energy efficiency, are branches 2-3 and 3-4. Though branch 2-3 has slightly lower energy efficiency than branch 3-4, the latter is selected to be isolated as the former is critical branch in order for keeping all the network parts interconnected. The preferred network topology after removing branches 2-4 and 3-4 looks like as shown in Fig 3.

On the other hand, based on the values of heating network parameters found from the load flow analysis, the exergy loss across each branch are calculated as shown in Table 4. The exergy loss calculation for each pipe considers the exergy destruction due to heat loss and pressure drop. The exergy loss associated with the pressure drop across each pipe is

equivalent to the exergy input by the corresponding circulation pump (i.e. We/2, see equation (9)). The effect of friction on increasing the water temperature is neglected in this study. As it can be seen from Table 4, the branch 2-4 has the lowest exergy efficiency followed by branches 3-4 and 2-3. Isolating branches 2-4 and 3-4 results in a similar topology as in Fig 3.

*Table 2: Load flow results at node level – Scenario I*

| Hub | Pepg (kW) | Phg (kW) | HP_e (kW) | Lh (kW) | m(kg/s) | Ts | Tr | Hs (m) | Hr(m) |
|---|---|---|---|---|---|---|---|---|---|
| **1** | 40.0231 | 99.746 | 0 | 0 | 0.453 | 85.000 | 32.361 | 10.000 | 6.000 |
| **2** | 0 | 0 | 0 | 100 | -0.638 | 72.455 | 35.000 | 8.948 | 7.052 |
| **3** | 0 | 160 | 40 | 0 | 0.693 | 85.000 | 29.846 | 9.130 | 6.870 |
| **4** | 0 | 0 | 0 | 100 | -0.567 | 77.166 | 35.000 | 8.952 | 7.048 |
| **5** | 40 | 160 | 40 | 0 | 0.717 | 85.000 | 31.672 | 11.384 | 4.616 |
| **6** | 0 | 0 | 0 | 100 | -0.658 | 71.301 | 35.000 | 8.445 | 7.555 |

*Table 3: Load flow results of the DHN at branch level – Scenario I*

| Nodes | | Flow | Supply Pipe Network of DHN | | | | Return Pipe Network of DHN | | | | Branch i to j | | | |
|---|---|---|---|---|---|---|---|---|---|---|---|---|---|---|
| ***i*** | ***j*** | *(kg/s)* | *$H_i$ (m)* | *$H_j$ (m)* | *Tsi (°C)* | *Tsj (°C)* | *$H_i$ (m)* | *$H_j$ (m)* | *Tri (°C)* | *Trj (°C)* | *We (kW)* | *Net heat flow (kW)* | *Loss (kW)* | *Efficiency %* |
| **1** | 2 | 0.453 | 10.00 | 8.948 | 85.000 | 77.082 | 6.00 | 7.052 | 32.361 | 35.00 | 0.0117 | 79.74 | 20.0 | 79.94 |
| **2** | 4 | -0.016 | 8.948 | 8.952 | 13.017 | 77.166 | 7.05 | 7.048 | 35.000 | 11.12 | 0.0000 | 0.00 | 5.87 | 0.00 |
| **2** | 3 | -0.169 | 8.948 | 9.130 | 65.668 | 85.000 | 7.05 | 6.870 | 35.000 | 28.56 | 0.0008 | -21.72 | 18.3 | 54.33 |
| **3** | 4 | 0.167 | 9.130 | 8.952 | 85.000 | 65.461 | 6.87 | 7.048 | 27.197 | 33.26 | 0.0007 | 22.53 | 17.9 | 55.72 |
| **3** | 6 | 0.357 | 9.130 | 8.445 | 85.000 | 75.099 | 6.87 | 7.555 | 31.700 | 35.00 | 0.0060 | 59.87 | 19.7 | 75.23 |
| **4** | 5 | -0.717 | 8.952 | 11.38 | 79.895 | 85.000 | 7.05 | 4.616 | 33.255 | 31.67 | 0.0427 | -139.9 | 20.1 | 87.46 |
| **4** | 6 | 0.301 | 8.952 | 8.445 | 77.166 | 66.807 | 7.05 | 7.555 | 31.144 | 35.00 | 0.0037 | 40.13 | 17.9 | 69.11 |

*Table 4: Exergy of water at the inlet and outlet of branch pipes and associated losses – Scenario I*

| Nodes | | Exergy of pipe on the supply side (kW) | | | | Exergy of pipe on the return side (kW) | | | | Branch i to j | | |
|---|---|---|---|---|---|---|---|---|---|---|---|---|
| ***i*** | ***j*** | *At node i* | *At node j* | *loss* | *Exergy efficiency* | *At node i* | *At node j* | *loss* | *Exergy efficiency* | *Net exergy flow (kW)* | *Exergy lost (kW)* | *Exergy efficiency* |
| **1** | 2 | 16.447 | 13.391 | 3.06 | 81.39% | 1.812 | 2.245 | 0.433 | 80.51% | 13.391 | 3.489 | 79.27% |
| **2** | 4 | 0.013 | 0.472 | 0.46 | 2.85% | 0.079 | 0.010 | 0.069 | 12.14% | 0.013 | 0.528 | 2.49% |
| **2** | 3 | 3.566 | 6.134 | 2.57 | 58.13% | 0.839 | 0.510 | 0.329 | 60.77% | 3.566 | 2.897 | 55.17% |
| **3** | 4 | 6.058 | 3.498 | 2.56 | 57.74% | 0.447 | 0.733 | 0.285 | 61.02% | 3.498 | 2.846 | 55.14% |
| **3** | 6 | 12.928 | 9.973 | 2.96 | 77.12% | 1.387 | 1.786 | 0.399 | 77.51% | 9.973 | 3.355 | 74.79% |
| **4** | 5 | 22.847 | 26.139 | 3.29 | 87.33% | 3.143 | 2.622 | 0.521 | 82.87% | 22.847 | 3.813 | 85.56% |
| **4** | 6 | 8.937 | 6.575 | 2.36 | 73.55% | 1.128 | 1.509 | 0.382 | 74.63% | 6.575 | 2.744 | 70.53% |

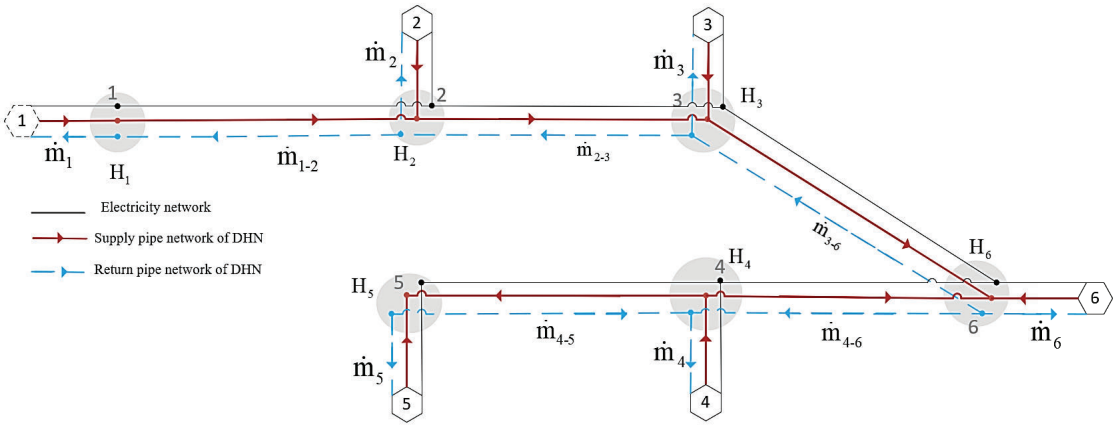


*Fig. 3 The reduced network topology after isolating the lossy branches*

*Table 5: Exergy flow to/from the environment and exergy efficiency at each node – Scenario I*

| Exergy on supply side nodes (kW) | | | | Exergy on return side nodes (kW) | | | Nodal exergy efficiency |
|---|---|---|---|---|---|---|---|
| *Node* | *External input* | *Total input* | *Total output* | *External input* | *Total input* | *Total output* | |
| **1** | 16.447 | 16.447 | 16.447 | -1.812 | 1.812 | 1.812 | 100.00% |
| **2** | -16.567 | 16.970 | 16.567 | 3.163 | 3.163 | 3.163 | 98.00% |
| **3** | 25.120 | 25.120 | 25.120 | -2.327 | 2.344 | 2.327 | 99.94% |
| **4** | -16.798 | 26.345 | 26.206 | 2.809 | 3.947 | 3.876 | 99.31% |
| **5** | 26.139 | 26.139 | 26.139 | -2.622 | 2.622 | 2.622 | 100.00% |
| **6** | -16.491 | 16.547 | 16.491 | 3.296 | 3.296 | 3.296 | 99.72% |

The exergy destruction at each node due to the irreversibility of mixing of water at different temperature is calculated by taking all the input and output exergy flows both on supply and return nodes. A complete mixing of water is assumed at all nodes. Each node represented by the grey circle in Fig 1 has two physically separated thermal nodes: one on the supply side and the other on the return side of the DHN. Any heat flow from/to external environment is also treated as two separate flows, i.e. one on the supply side and the other on the return side with opposite direction of flow. The nodal exergy efficiencies, considering both supply and return nodes, are shown in Table 5. Node 2 has the lowest nodal efficiency due to the mixing of three flows at different temperatures on the supply side. On the other hand, nodes 1 and 5 are at 100% efficiency because of having a single mass flow going into the node. It can be concluded that the nodal exergy destructions are negligible compared to the branch exergy destructions. The total exergy input and output of the DHN are calculated to be 77.04kW and 56.62kW, respectively. In other words, about 20.36kW of exergy is destroyed in the DHN giving a DHN exergy efficiency of 73.49%.

After running the load flow simulation with the reduced topology (i.e. Scenario II), the heat loss is reduced to 92.62kW giving a DHN energy efficiency of 75.64%. The detailed results of the load flow are summarised in Tables 5 and 6. The loss in the electricity distribution network is about 0.028kW (0.036% of the demand) which is slightly higher than the loss in Scenario I.

*Table 6: Load flow results at node level - Scenario II*

| Hub | Pelg(kW) | Phg (kW) | HP_e (kW) | Lh (kW) | m(kg/s) | Ts | Tr | Hs (m) | Hr(m) |
|---|---|---|---|---|---|---|---|---|---|
| **1** | 40.028 | 76.622 | 0 | 0 | 0.343 | 85.000 | 31.574 | 10.000 | 6.000 |
| **2** | 0 | 0 | 0 | 100 | -0.618 | 73.694 | 35.000 | 9.363 | 6.637 |
| **3** | 0 | 160 | 40 | 0 | 0.718 | 85.000 | 31.730 | 9.792 | 6.208 |
| **4** | 0 | 0 | 0 | 100 | -0.532 | 79.914 | 35.000 | 9.000 | 7.000 |
| **5** | 40 | 160 | 40 | 0 | 0.720 | 85.000 | 31.872 | 11.449 | 4.551 |
| **6** | 0 | 0 | 0 | 100 | -0.630 | 72.900 | 35.000 | 8.781 | 7.219 |

*Table 7: Load flow results of the DHN at branch level – Scenario II*

| **Nodes** | | **Flow** | **Supply Pipe Network of DHN** | | | | **Return Pipe Network of DHN** | | | | **Branch i to j** | | | |
|---|---|---|---|---|---|---|---|---|---|---|---|---|---|---|
| **i** | *j* | *(kg/s)* | $H_i$ *(m)* | $H_j$ *(m)* | *Tsi (°C)* | *Tsj (°C)* | $H_i$ *(m)* | $H_j$ *(m)* | *Tri (°C)* | *Trj (°C)* | *We (kW)* | *Net heat flow (kW)* | *Loss (kW)* | *Efficiency %* |
| **1** | 2 | 0.343 | 10.0 | 9.36 | 85.00 | 74.723 | 6.00 | 6.64 | 31.574 | 35.00 | 0.005 | 56.97 | 19.65 | 74.35 |
| **2** | 3 | -0.275 | 9.36 | 9.79 | 72.41 | 85.000 | 6.64 | 6.21 | 35.000 | 30.80 | 0.003 | -43.03 | 19.30 | 69.03 |
| **3** | 6 | 0.443 | 9.79 | 8.78 | 85.00 | 76.915 | 6.21 | 7.22 | 32.305 | 35.00 | 0.011 | 77.69 | 19.98 | 79.54 |
| **4** | 5 | -0.720 | 9.00 | 11.45 | 79.91 | 85.000 | 7.00 | 4.55 | 33.463 | 31.87 | 0.043 | -139.89 | 20.11 | 87.43 |
| **4** | 6 | 0.188 | 9.00 | 8.78 | 79.91 | 63.424 | 7.00 | 7.22 | 29.103 | 35.00 | 0.001 | 22.31 | 17.58 | 55.94 |

*Table 8: Exergy of water at the inlet and outlet of branch pipes and associated losses – Scenario II*

| **Node** | | **Exergy of pipe on the supply side (kW)** | | | | **Exergy of pipe on the return side (kW)** | | | | **Branch i to j** | | |
|---|---|---|---|---|---|---|---|---|---|---|---|---|
| ***i*** | ***j*** | ***At node i*** | ***at node j*** | ***loss*** | Exergy efficiency | ***At node i*** | ***At node j*** | ***loss*** | Exergy efficiency | Net exergy flow (kW) | Exergy lost (kW) | Exergy efficiency |
| **1** | 2 | 12.45 | 9.510 | 2.94 | 76.38% | 1.290 | 1.685 | 0.398 | 76.44% | 9.510 | 3.344 | 73.99% |
| **2** | 3 | 7.14 | 9.977 | 2.84 | 71.54% | 1.351 | 0.979 | 0.373 | 72.34% | 7.139 | 3.217 | 68.94% |
| **3** | 6 | 16.08 | 13.031 | 3.05 | 81.02% | 1.774 | 2.203 | 0.435 | 80.32% | 13.031 | 3.498 | 78.84% |
| **4** | 5 | 22.95 | 26.242 | 3.3 | 87.37% | 3.199 | 2.670 | 0.550 | 82.92% | 22.947 | 3.910 | 85.44% |
| **4** | 6 | 5.98 | 3.664 | 2.32 | 61.25% | 0.595 | 0.933 | 0.339 | 63.69% | 3.664 | 2.658 | 57.95% |

*Table 9: Exergy flow to/from the environment and exergy efficiency at each node– Scenario II*

| **Exergy on supply side nodes (kW)** | | | | **Exergy on return side nodes (kW)** | | | **Nodal exergy efficiency** |
|---|---|---|---|---|---|---|---|
| *Node* | *External input* | *Total input* | *Total output* | *External input* | *Total input* | *Total output* | |
| **1** | 12.448 | 12.448 | 12.448 | -1.290 | 1.290 | 1.290 | 100.00% |
| **2** | -16.645 | 16.649 | 16.645 | 3.036 | 3.036 | 3.036 | 99.98% |
| **3** | 26.055 | 26.055 | 26.055 | -2.750 | 2.752 | 2.750 | 99.99% |
| **4** | -16.965 | 22.947 | 22.947 | 2.635 | 3.229 | 3.199 | 99.88% |
| **5** | 26.242 | 26.242 | 26.242 | -2.670 | 2.670 | 2.670 | 100.00% |
| **6** | -16.575 | 16.695 | 16.575 | 3.136 | 3.136 | 3.136 | 99.40% |

The exergy destruction at branch and node levels for Scenario II are summarised in Tables 8 and 9, respectively. The lowest branch exergy efficiency in Scenario II is about 57.97% which is much higher when compared to that of Scenario I (which is 2.49%). There is no significant difference in the nodal efficiencies, except a slight improvement at node 2 due to the decrease in the number of mixing flows from 3 in Scenario I to 2 in Scenario II.

The total exergy input and output of the DHN for Scenario II are 73.62kW and 56.89kW, respectively, with an exergy efficiency of 77.29%. This shows that Scenario II has slightly higher efficiency for the same amount of loading and HP sizes. Considering the prices of 0.20€/kWh of electricity from the grid and 0.10 €/kWh of heat from neighbourhood, it is found that the total operating cost of the DHN before isolating lossy branches (Scenario I) is calculated to be 17.99€/h. After the lossy branches are isolated (Scenario II), the operating cost is reduced to 15.68€/h.

### *4.2. Thermo-economic optimization (Scenarios III & IV)*

Scenario III is the application of PSO on the reduced topology (Fig. 2) with the consideration of all the constraints discussed in Section 2.3 and Section 3. The load flow results of the DHN after running the PSO on Scenario III are shown in Tables 10 and 11. As it can be seen from Table 10, the PSO selected HPs at Hubs 2, 4 and 6 to operate at 25kWe, each of them producing 100kW. The produced heat is equal to the heat demand at the corresponding hub. The HPs at Hubs 3 and 5 are set at zero. Although there is free electricity at Hub5, the corresponding HP is not selected by the PSO. It means that the electricity is transported to and used by HPs at the other hubs. In other words, the PSO found that the cost of transporting heat from Hub 5 is higher than the cost of transporting electricity from the same hub. As all the heat demands are met locally at each hub, the nodal and pipe mass flows are zero. Thus, there is no thermal exergy flow and no heat loss in the DHN (see Table 11). The DHN is at 100% of energy efficiency. The loss in the electric distribution network is 0.029kW which is about 0.038% of the electricity demand by the HPs (i.e. 75kW). The operating cost of the DHN is 7.005€/h which shows a 55% reduction compared to Scenario I.

The optimization is repeated on Scenario IV (unbalanced loading of hubs made by shifting 40kW of load from Hub 4 to Hub 6 while keeping the total demand at the same value of 300kW). The results are shown in Tables 12 – 15. The total cost has increased slightly to 8.35€/h compared to Scenario III. The HP at Hubs 2 is selected in Scenario IV to run at its full capacity producing 100kW of heat which is equal to the heat demand at the same hub. The HP at Hub 6 is also selected to produce 100kW of heat at full capacity. However, the demand at this hub is 40kW more than what is produced. The offset has to be met by heat generated at the other hubs. The HP at Hub 4, on the other hand, could have been set to generate only 60kW of heat. But, the PSO compared cost of production, loss in the transportation and capacity limits and selected HP at Hub 4 to run at its maximum capacity producing extra 40kW of heat than its demand. This heat is transported to Hub 6. As there is loss associated with the transport, additional heat power generation is required to compensate it. There are three options for this: running HP at Hub 3, running HP at Hub 5 and importing heat from Hub 1. HP at Hub 5 is selected by the PSO as there is a local generation of electricity at this hub. This will avoid the additional loss in the electric network that could have been incurred if the HP at Hub 3 was selected. It should also be noted that the size of the HP at Hub 5 is not at its maximum capacity. The reason could be associated to the cost of the possible heat loss in the heating network while transporting the heat produced. Generally speaking, supplying demands from locally available sources helps to decrease the loss in the network. HPs are demands from the electric network and sources from the heating network point of views. Their optimization is, therefore, affected by the possible losses in both networks.

The total heat lost in the network in Scenario IV is 26.8kW which implies a DHN energy efficiency of 91.8%. The power lost in the electric network is about 0.031kW which is about 0.038% of the demand by the HPs (i.e. 81.701kW). The total

exergy input and output of the DHN are 15.16kW and 6.43kW, respectively, with an exergy efficiency of 42.42%. This shows that although the DHN is running at a lower exergy efficiency, the overall system is running at a lower cost due to the fact that very low amount of exergy is flowing through the network in comparison to Scenarios I and II.

*Table 10: Load flow results at node level – Scenario III*

| Hub | Pelg (kW) | Phg (kW) | HP_e (kW) | Lh (kW) | m(kg/s) | Ts | Tr | Hs (m) | Hr(m) |
|---|---|---|---|---|---|---|---|---|---|
| **1** | 35.029 | 0 | | 0 | -8.46E-17 | 12.70 | 12.70 | 10.00 | 6.00 |
| **2** | 0.000 | 100 | 25 | 100 | 5.54E-17 | 90.02 | 33.67 | 10.00 | 6.00 |
| **3** | 0.000 | 0 | 0 | 0 | 0 | 90.74 | 33.92 | 10.00 | 6.00 |
| **4** | 0.000 | 100 | 25 | 100 | 6.25E-18 | 90.74 | 10.30 | 10.00 | 6.00 |
| **5** | 40.000 | 0 | 0 | 0 | -4.19E-35 | 63.35 | 30.00 | 10.00 | 6.00 |
| **6** | 0.000 | 100 | 25 | 100 | 2.29E-17 | 65.00 | 30.00 | 10.00 | 6.00 |

*Table 11: Load flow results of DHN at branch level – Scenario III*

| Nodes | | Flow | Supply Pipe Network of DHN | | | | Return Pipe Network of DHN | | | | Branch i to j | | | |
|---|---|---|---|---|---|---|---|---|---|---|---|---|---|---|
| **i** | *j* | *(kg/s)* | *$H_i$ (m)* | *$H_j$ (m)* | *Ts i (°C)* | *Ts j (°C)* | *$H_i$ (m)* | *$H_j$ (m)* | *Tr_i (°C)* | *Tr_j (°C)* | *We (kW)* | *Net heat flow (kW)* | *Loss (kW)* | *Efficiency %* |
| **1** | 2 | 0.00 | 10.0 | 10.0 | 10.00 | 92.073 | 6.00 | 6.000 | 10.000 | 10.000 | 0.00 | 0.00 | 0.00 | -- |
| **2** | 3 | 0.00 | 10.0 | 10.0 | 10.00 | 10.000 | 6.00 | 6.000 | 17.140 | 10.000 | 0.00 | 0.00 | 0.00 | -- |
| **3** | 6 | 0.00 | 10.0 | 10.0 | 10.00 | 20.177 | 6.00 | 6.000 | 10.000 | 10.000 | 0.00 | 0.00 | 0.00 | -- |
| **4** | 5 | 0.00 | 10.0 | 10.0 | 10.00 | 10.000 | 6.00 | 6.000 | 10.000 | 10.000 | 0.00 | 0.00 | 0.00 | -- |
| **4** | 6 | 0.00 | 10.0 | 10.0 | 71.73 | 10.000 | 6.00 | 6.000 | 10.000 | 10.000 | 0.00 | 0.00 | 0.00 | -- |

*Table 12: Load flow results at node level – Scenario IV*

| Hub | Pelg (kW) | Phg (kW) | HP_e (kW) | Lh (kW) | m(kg/s) | Ts | Tr | Hs (m) | Hr(m) |
|---|---|---|---|---|---|---|---|---|---|
| **1** | 41.731 | 0.000 | 0.000 | 0.00 | 0.00000 | 10.000 | 10.000 | 10.000 | 6.000 |
| **2** | 0.00 | 100.000 | 25.000 | 100.00 | 0.00000 | 65.000 | 10.000 | 10.000 | 6.000 |
| **3** | 0.00 | 0.000 | 0.000 | 0.00 | 0.00000 | 65.000 | 10.000 | 10.000 | 6.000 |
| **4** | 0.00 | 100.000 | 25.000 | 60.00 | 0.25601 | 65.000 | 27.666 | 10.869 | 5.131 |
| **5** | 40.00 | 26.802 | 6.701 | 0.00 | 0.15125 | 65.000 | 22.657 | 11.018 | 4.982 |
| **6** | 0.00 | 100.000 | 25.000 | 140.00 | -0.40729 | 53.467 | 30.000 | 10.000 | 6.000 |

*Table 13: Load flow results at branch level – Scenario IV*

| Nodes | | Flow | Supply Pipe Network of DHN | | | | Return Pipe Network of DHN | | | | Branch i to j | | | |
|---|---|---|---|---|---|---|---|---|---|---|---|---|---|---|
| **i** | *j* | *(kg/s)* | *$H_i$ (m)* | *$H_j$ (m)* | *Ts i (°C)* | *Ts j (°C)* | *$H_i$ (m)* | *$H_j$ (m)* | *Tr_i (°C)* | *Tr_j (°C)* | *We (kW)* | *Net heat flow (kW)* | *Loss (kW)* | *Efficiency %* |
| **1** | 2 | 0.000 | 10.000 | 10.000 | 10.000 | 10.00 | 6.00 | 6.000 | 10.0 | 10.00 | 0.000 | 0.00 | 0.0 | -- |
| **2** | 3 | 0.000 | 10.000 | 10.000 | 10.000 | 10.00 | 6.00 | 6.000 | 10.000 | 10.00 | 0.000 | 0.00 | 0.0 | -- |
| **3** | 6 | 0.000 | 10.000 | 10.000 | 10.000 | 10.00 | 6.00 | 6.000 | 10.00 | 30.00 | 0.000 | 0.00 | 0.0 | -- |
| **4** | 5 | -0.151 | 10.869 | 11.018 | 49.402 | 65.00 | 5.13 | 4.982 | 27.66 | 22.66 | 0.001 | -13.76 | 13.1 | 51.33 |
| **4** | 6 | 0.407 | 10.869 | 10.000 | 59.207 | 53.47 | 5.13 | 6.000 | 27.67 | 30.00 | 0.009 | 40.00 | 13.8 | 74.39 |

*Table 14: Exergy of water at the inlet and outlet of branch pipes and associated losses – Scenario IV*

| Node | | Exergy of pipe on the supply side (kW) | | | | Exergy of pipe on the return side (kW) | | | | Branch i to j | | |
|---|---|---|---|---|---|---|---|---|---|---|---|---|
| ***i*** | j | At node i | At node j | loss | Exergy efficiency | At node i | At node j | loss | Exergy efficiency | Net exergy flow (kW) | Exergy lost (kW) | Exergy efficiency |
| **1** | 2 | 0.000 | 0.000 | 0.000 | -- | 0.000 | 0.000 | 0.00 | -- | 0.000 | 0.000 | -- |
| **2** | 3 | 0.000 | 0.000 | 0.000 | -- | 0.000 | 0.000 | 0.00 | -- | 0.000 | 0.000 | -- |
| **3** | 6 | 0.000 | 0.000 | 0.000 | -- | 0.000 | 0.000 | 0.00 | -- | 0.000 | 0.000 | -- |
| **4** | 5 | 1.736 | 3.148 | 1.412 | 55.15% | 0.396 | 0.233 | 0.16 | 58.76% | 1.736 | 1.576 | 52.42% |
| **4** | 6 | 6.936 | 5.525 | 1.415 | 79.61% | 1.067 | 1.350 | 0.29 | 78.79% | 5.525 | 1.711 | 76.35% |

*Table 15: Exergy flow to/from the environment and the exergy efficiency at each node– Scenario IV*

| | Exergy on supply side nodes (kW) | | | Exergy on return side nodes (kW) | | | Nodal exergy efficiency |
|---|---|---|---|---|---|---|---|
| *Node* | *External input* | *Total input* | *Total output* | *External input* | *Total input* | *Total output* | |
| **1** | 0.000 | 0.000 | 0.000 | 0.000 | 0.000 | 0.000 | -- |
| **2** | 0.000 | 0.000 | 0.000 | 0.000 | 0.000 | 0.000 | -- |
| **3** | 0.000 | 0.000 | 0.000 | 0.000 | 0.000 | 0.000 | -- |
| **4** | 5.325 | 7.061 | 6.936 | -0.671 | 1.067 | 1.067 | 98.46% |
| **5** | 3.148 | 3.148 | 3.148 | -0.233 | 0.233 | 0.233 | 100.00% |
| **6** | -5.525 | 5.525 | 5.525 | 1.350 | 1.350 | 1.350 | 100.00% |

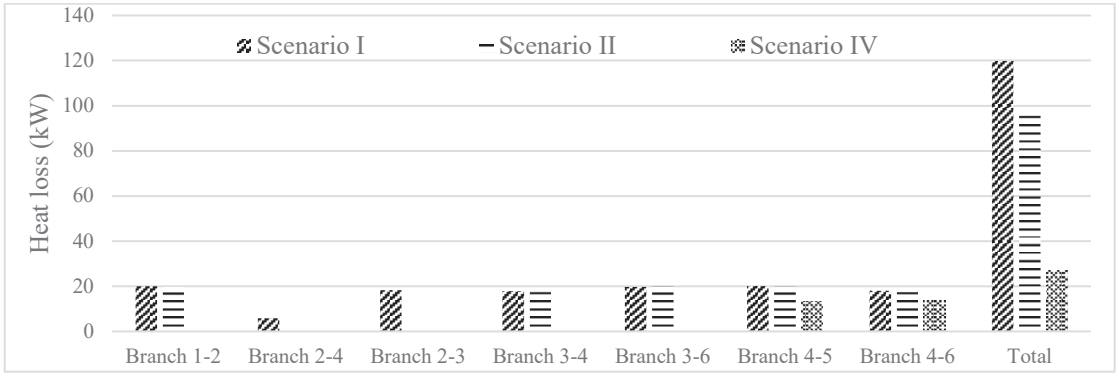


*Fig. 4 Comparison of exergy losses on the branch different operating scenarios*

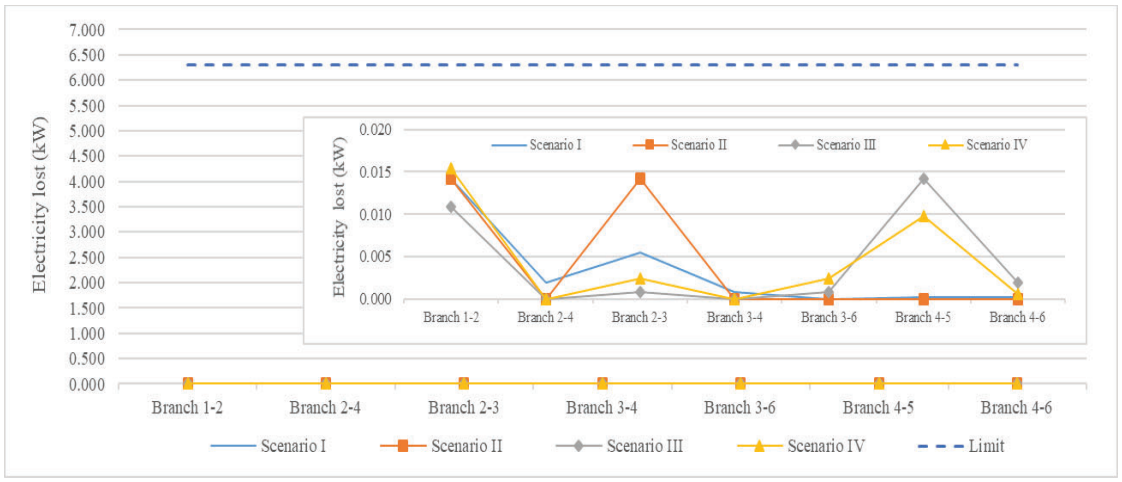


*Fig. 5 Electric power lost in each branch for different scenarios*

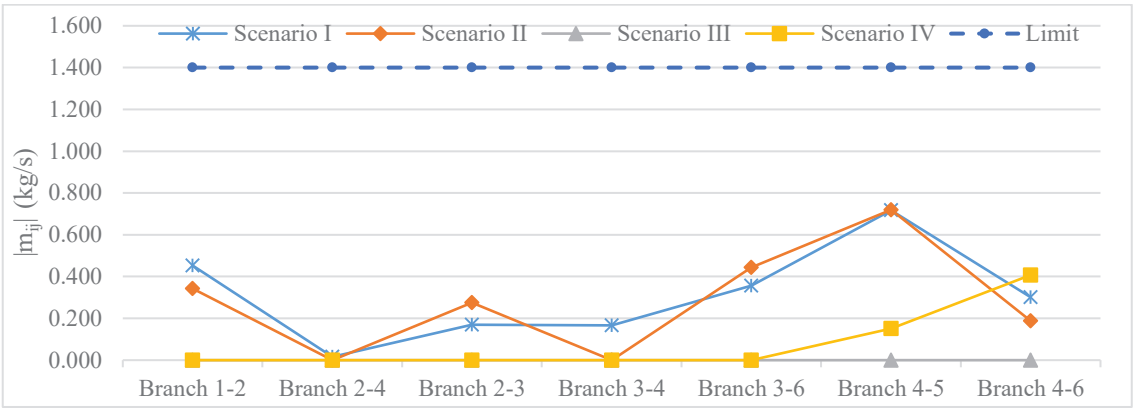


*Fig. 6 The magnitude of mass flow in each branch for different scenarios*

Figure 4 shows the exergy losses of the seven branches for Scenarios I, II and IV. Scenario III is not included as all the network flows and, hence, the corresponding heat losses are zero. From Fig. 4, it can be observed that the loss in branch 3-4 is higher in Scenario II than I, but the total heat loss is lower in Scenario II. From the four scenarios, the third scenario has the lowest (zero) heat loss in the network which is followed by Scenarios IV, II and I.

Figures 5 and 6 show the electric power losses and branch mass flows with respect to their limits, respectively. It can be observed that the branch flows in both of the electric and heating networks are within their limits. Figure 7 shows the nodal voltage profiles in per unit. All of the voltage magnitudes are nearly equal to 1pu. It means that the voltage drop on the branches is almost zero. This is because of the assumption of a unity power factor for each HP which implies a

zero reactive power demand. Hence, only active power flow is required in the network. Active power flows are highly dependent on voltage angles and are less dependent on voltage magnitude unlike to reactive power flows. As a result, the voltage magnitude variations are negligible as shown in Fig 7.

The supply temperatures at different hubs for different scenarios are shown in Fig 8. The supply temperature at different hubs for Scenarios I and II are within the limits. For Scenario III, nodal mass flows from all hubs are nearly zero (see Table 10). Thus, equation (12d) is not binding. In the case of Scenario IV, the supply temperatures at Hubs 2, 3, 4 and 5 are found to be equal to 65℃ which is the lower possible value. As Hub 1 has zero mass flow and Hub 6 is acting as a heat consumer, equation (12d) is not binding for them. So, the supply temperature profiles for all scenarios satisfy the inequality constraint defined in (12d).

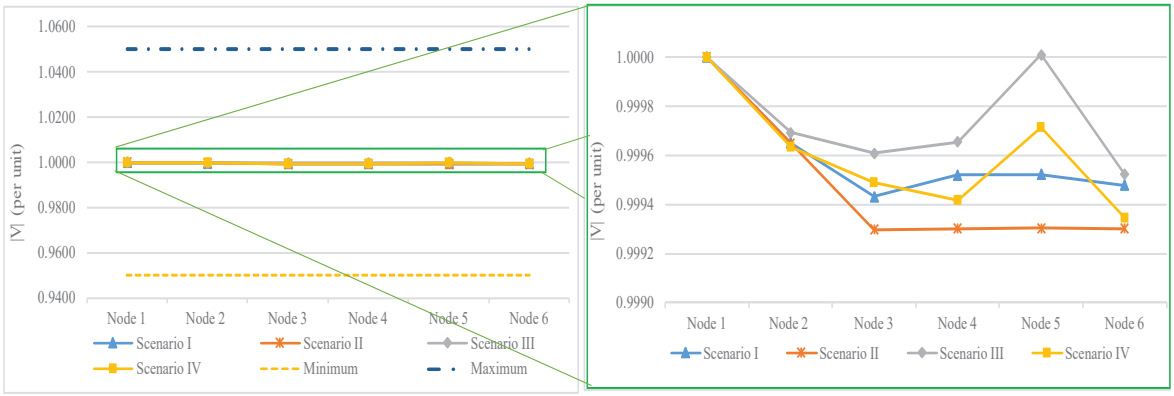


*Fig. 7 Voltage magnitude in per unit at different nodes for different scenarios*

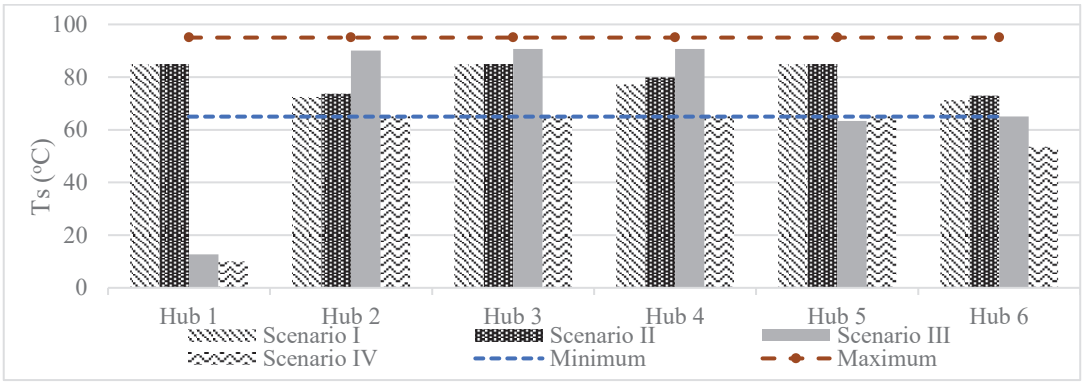


*Fig. 8 Supply temperature at different hubs for different scenarios*

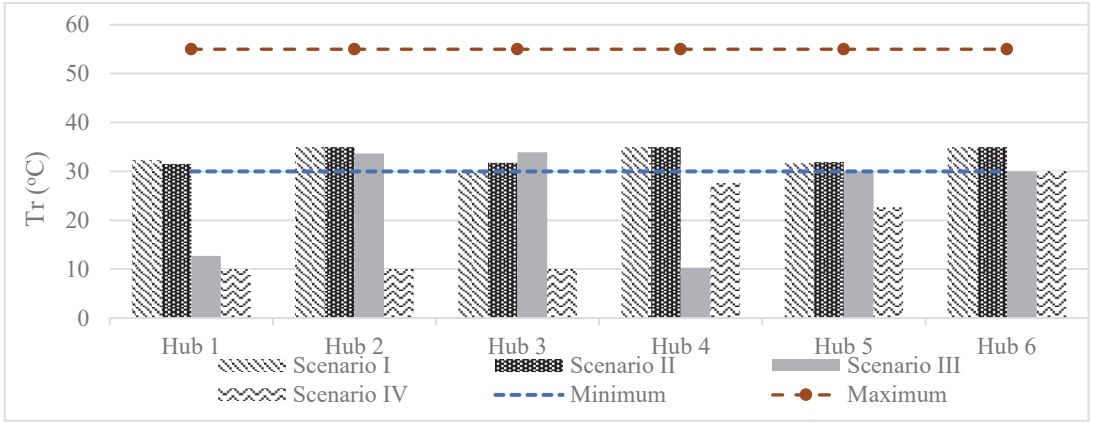


*Fig. 9 Return temperature at different hubs for different scenarios*

Figure 9, on the other hand, shows the return temperature profiles at different hubs for the four scenarios. As it shown in the figure, Scenarios I and II are within the limit. As the nodal mass flows are almost zero in Scenario III, the constraint in (12e) is not binding. In the case of Scenario IV, only Hub 6 is acting as a heat consumer with a negative nodal mass flow. The return temperature at this hub is 30°C, which is the lowest possible value. Other hubs have either zero or positive nodal mass flows (see Table 12) and, hence, the constraint (12e) is not binding for them. Thus, the return temperature inequality constraint of (12e) is satisfied at all hubs for all scenarios.

## 5. Conclusion

The network topology optimization based on branch efficiency showed that both of the energy and exergy analyses could result in the same reduced network topology. If exergy analysis is applied on DHN with the full consideration of temperature, mass flows and hydraulic heads, it could give a better clarity in identifying the lossy branches and nodes of thermal networks. Significant amount of exergy destruction takes place across the branches, rather than at the nodes. It has also been found that the contribution of the return pipe network in the exergy loss is indispensable, though it is much lower than the supply side pipe networks. On the other hand, exergy analysis is based on the load flow results which are computed on energy basis. Furthermore, energy analysis can be further combined with thermo-economic optimization using heuristic algorithms, such as Particle Swarm Optimization, in order to decrease operational costs of the reduced topology of the DHN. The optimization results show that distributed heat pumps are more economical than the neighbourhood DHN for the given load profile and price signals. However, the optimality of each HP highly depends on the system heat demand profiles and the relative location of each HP from the nearby heat load and from the nearby electricity generation plant. It also depends on the cost of electricity and heat in the neighbourhood and the coupling technology used. In general, avoiding the heating network, if possible, or running it at a lower possible temperature profile is found to have the lowest operational cost. In other words, HPs near to the thermal load are usually the first priority to run. If two similar HPs are far from the heat load, as is the case for HPs at Hubs 3 and 5 of scenario IV, then the HP which is located to cheaper electricity generation plant gets a priority. Thus, consideration of the electricity network model is very important in order to arrive at an optimal operation strategy of a district energy system consisting of coupling technologies such as HPs.

The methodology developed in this paper can be applied on different combinations of energy carriers, distributed generations, coupling technologies and thermal storage. The exergy analysis covered in this study is limited to only at DHN level. It can be complemented by considering the exergy interaction between different energy carriers inside the energy hubs. The COP of each HP is also assumed to be equal for partial and full load running. This could be improved by incorporating a model for partial loading COP of a HP. Electricity demands with both active and reactive loads together with CHPs and HPs with lagging power factors can also be considered to study the capacity of the electricity distribution network. The sensitivity of the optimal solutions can also be further investigated by considering a range of prices for different energy carriers, such as gas, fuel, electricity and heat. Optimization algorithms other than PSO can also be applied for comparative study.

**Acknowledgments**

The research presented is performed within the framework of the Erasmus Mundus Joint Doctorate SELECT+ program ‘Environomical Pathways for Sustainable Energy Services’ and funded with support from the Education, Audiovisual, and Culture Executive Agency (EACEA) (FPA-2012-0034) of the European Commission. This publication reflects the views only of the author(s), and the Commission cannot be held responsible for any use, which may be made of the information contained therein.

## Nomenclatures

| | |
|---|---|
| B | Susceptance of transmission line (S) |
| $B_{ph}$ | Physical exergy (W) |
| $c_1$ | Personal acceleration factor |
| $c_2$ | Global acceleration factor |
| $C_p$ | Specific heat capacity of water (J/Kkg) |
| CHP | Combined heat and power |
| COP | Coefficient of performance |
| D, $D_1$ | Internal diameter of a pipe (m) |
| D3 | Outer diameter of insulating material(m) |
| DHN | District Heating Network |
| $\Delta T$ | Temperature difference (K) |
| e | Internal surface roughness of a pipe (m) |
| H | Hydraulic head (m) |
| HP | Heat pump |
| HP_e | Electricity consumption of HP (W) |
| K | Pressure resistance coefficient ($m.s^2/kg^2$) |
| L | Length (m) |
| $L_h$ | Heat power demand (W) |
| $L_{Pel}$ | Active electric power demand (W) |
| $L_{Qel}$ | Reactive electric power demand (var) |
| $\dot{m}$ | Mass flow rate from a hub (kg/s) |
| $\dot{m}_{ij}$ | Mass flow rate from node i to j (kg/s) |
| $P_{el}$ | Active electric power injection (W) |
| $P_{elg}$ | Active electric power generated (W) |
| $P_h$ | Heat power injection (W) |
| $P_{hg}$ | Heat power generated (W) |
| $P$ | Pressure of water (Pa) |
| $P_o$ | Reference pressure (Pa) |
| $Q_{el}$ | Reactive power injection (var) |
| $Q_{elg}$ | Reactive power generated (var) |
| R | Resistance of a transmission line (Ω) |
| T | Temperature (K) |
| $t_1$ | Thickness of carrier pipe (m) |
| $t_3$ | Thickness of outer jacket (m) |
| $T_o$ | Reference temperature (K) |
| V | voltage (V) |
| $v_{i-new}$ | new velocity of particle *i* |
| $v_{io}$ | current velocity of particle *i* |
| $W_e$ | electricity used for circulation pumps (W) |
| X | Reactance of a transmission line (Ω) |
| $x_i$ | current position of particle *i* |
| $x_{i-new}$ | new position of particle *i* |
| $x_{i-best}$ | Best position of particle *i* |
| $x_{g-best}$ | Global best position |
| $Z$ | Depth of pipe from the boundary surface to the centre of pipe (m) |
| $\omega$ | inertia factor |

**Subscripts**

| | |
|---|---|
| i, j, k | Hub numbers |
| r | Return pipe of DHN |
| s | Supply pipe of DHN |

## Appendices

### A: Branch parameters

*Table A-1: Pipe parameters in the heating network and transmission line parameters in the electricity network*

| **Hubs** | | **Carrier Pipe Parameters** | | | | | **Insulation** | | **Outer Jacket** | | **Transmission lines** | | | |
|---|---|---|---|---|---|---|---|---|---|---|---|---|---|---|
| ***from*** | *to* | *L (m)* | *$D_1 + t_1$ (mm)* | *$t_1$ (mm)* | *$k_2$ (W/mK)* | *e (mm)* | *$k_3$ (W/mK)* | *$D_3$ (mm)* | *$t_3$ (mm)* | *$k_4$ (W/mK)* | *L (mi)* | *R (Ω/mi)* | *X (Ω/mi)* | *B (μS/mi)* |
| **1** | 2 | 1000 | 60.3 | 3.2 | 40 | 0.05 | 0.027 | 140 | 3.0 | 0.40 | 0.5 | 0.307 | 0.458 | 9.46 |
| **2** | 4 | 1000 | 60.3 | 3.2 | 40 | 0.05 | 0.027 | 140 | 3.0 | 0.40 | 0.5 | 0.307 | 0.458 | 9.46 |
| **3** | 2 | 1000 | 60.3 | 3.2 | 40 | 0.05 | 0.027 | 140 | 3.0 | 0.40 | 0.5 | 0.307 | 0.458 | 9.46 |
| **3** | 4 | 1000 | 60.3 | 3.2 | 40 | 0.05 | 0.027 | 140 | 3.0 | 0.40 | 0.5 | 0.307 | 0.458 | 9.46 |
| **4** | 5 | 1000 | 60.3 | 3.2 | 40 | 0.05 | 0.027 | 140 | 3.0 | 0.40 | 0.5 | 0.307 | 0.458 | 9.46 |
| **3** | 6 | 1000 | 60.3 | 3.2 | 40 | 0.05 | 0.027 | 140 | 3.0 | 0.40 | 0.5 | 0.307 | 0.458 | 9.46 |
| **4** | 6 | 1000 | 60.3 | 3.2 | 40 | 0.05 | 0.027 | 140 | 3.0 | 0.40 | 0.5 | 0.307 | 0.458 | 9.46 |

## References


[1] Frederiksen S, Werner S. District Heating and Cooling. Studentlitteratur AB; 2013.

[2] Bergman TL, Incropera FP, DeWitt DP, Lavine AS. Fundamentals of heat and mass transfer. John Wiley & Sons; 2011.

[3] Bejan A, Bejan, Moran, Tsatsaronis G, Moran M, Moran MJ, et al. Thermal Design and Optimization. John Wiley & Sons; 1996.

[4] Dincer I, Rosen MA. Exergy: Energy, Environment and Sustainable Development. Second Edition. Elsevier; 2013. doi:10.1016/B978-0-08-097089-9.00002-4.

[5] Yao E, Wang H, Wang L, Xi G, Maréchal F. Thermo-economic optimization of a combined cooling, heating and power system based on small-scale compressed air energy storage. Energy Conversion and Management 2016;118:377–86. doi:10.1016/j.enconman.2016.03.087.
[6] Wang J, Lu Y, Yang Y, Mao T. Thermodynamic performance analysis and optimization of a solar-assisted combined cooling, heating and power system. Energy 2016;115, Part 1:49–59. doi:10.1016/j.energy.2016.08.102.
[7] Bilgen E, Takahashi H. Exergy analysis and experimental study of heat pump systems. Exergy, An International Journal 2002;2:259–65. doi:10.1016/S1164-0235(02)00083-3.
[8] Curti V, von Spakovsky MR, Favrat D. An environomic approach for the modeling and optimization of a district heating network based on centralized and decentralized heat pumps, cogeneration and/or gas furnace. Part I: Methodology. International Journal of Thermal Sciences 2000;39:721–30. doi:10.1016/S1290-0729(00)00226-X.
[9] Terehovics E, Veidenbergs I, Blumberga D. Exergy Analysis for District Heating Network. Energy Procedia 2017;113:189–93. doi:10.1016/j.egypro.2017.04.053.
[10] Li H, Svendsen S. Energy and exergy analysis of low temperature district heating network. Energy 2012;45:237–46. doi:10.1016/j.energy.2012.03.056.
[11] Coss S, Guelpa E, Letournel E, Le-Corre O, Verda V, Coss S, et al. Formulation of Exergy Cost Analysis to Graph-Based Thermal Network Models. Entropy 2017;19:109. doi:10.3390/e19030109.
[12] HOMER - Hybrid Renewable and Distributed Generation System Design Software n.d. https://www.homerenergy.com/ (accessed November 5, 2018).
[13] Canada NR. RETScreen 2010. https://www.nrcan.gc.ca/energy/software-tools/7465 (accessed November 5, 2018).
[14] PowerWorld » The visual approach to electric power systems n.d. https://www.powerworld.com/ (accessed November 14, 2018).
[15] Nemati M, Braun M, Tenbohlen S. Optimization of unit commitment and economic dispatch in microgrids based on genetic algorithm and mixed integer linear programming. Applied Energy 2018;210:944–63. doi:10.1016/j.apenergy.2017.07.007.
[16] Subbaraj P, Rengaraj R, Salivahanan S. Enhancement of combined heat and power economic dispatch using self adaptive real-coded genetic algorithm. Applied Energy 2009;86:915–21. doi:10.1016/j.apenergy.2008.10.002.
[17] Niknam T, Azizipanah-Abarghooee R, Aghaei J. A new modified teaching-learning algorithm for reserve constrained dynamic economic dispatch. IEEE Transactions on Power Systems 2013;28:749–63. doi:10.1109/TPWRS.2012.2208273.
[18] Shabanpour-Haghighi A, Seifi AR, Niknam T. A modified teaching–learning based optimization for multi-objective optimal power flow problem. Energy Conversion and Management 2014;77:597–607. doi:10.1016/j.enconman.2013.09.028.
[19] Niknam T, Narimani MR, Aghaei J, Tabatabaei S, Nayeripour M. Modified Honey Bee Mating Optimisation to solve dynamic optimal power flow considering generator constraints. Transmission Distribution IET Generation 2011;5:989–1002. doi:10.1049/iet-gtd.2011.0055.
[20] Mazairac W, Salenbien R, Vries B de. Mixed-integer linear program for an optimal hybrid energy network topology. 2015 International Conference on Renewable Energy Research and Applications (ICRERA), 2015, p. 861–6. doi:10.1109/ICRERA.2015.7418533.
[21] Wang Y, Zhang N, Zhuo Z, Kang C, Kirschen D. Mixed-integer linear programming-based optimal configuration planning for energy hub: Starting from scratch. Applied Energy 2018;210:1141–50. doi:10.1016/j.apenergy.2017.08.114.
[22] Aote SS, Raghuwanshi MM, Malik LG. Improved Particle Swarm Optimization Based on Natural Flocking Behavior. Arab J Sci Eng 2016;41:1067–76. doi:10.1007/s13369-015-1990-5.
[23] Attous DB, Labbi Y. Particle swarm optimization based optimal power flow for units with non-smooth fuel cost functions. International Conference on Electrical and Electronics Engineering, 2009. ELECO 2009, 2009, p. I-377-I–381. doi:10.1109/ELECO.2009.5355329.
[24] Hazra J, Sinha AK. A multi-objective optimal power flow using particle swarm optimization. Euro Trans Electr Power 2011;21:1028–45. doi:10.1002/etep.494.
[25] Juneja M, Nagar SK. Particle swarm optimization algorithm and its parameters: A review. 2016 International Conference on Control, Computing, Communication and Materials (ICCCCM), 2016, p. 1–5. doi:10.1109/ICCCCM.2016.7918233.
[26] Ayele GT, Haurant P, Laumert B, Lacarrière B. An extended energy hub approach for load flow analysis of highly coupled district energy networks: Illustration with electricity and heating. Applied Energy 2018;212:850–67. doi:10.1016/j.apenergy.2017.12.090.
[27] Ayele GT, Mabrouk MT, Haurant P, Laumert B, Lacarrière B. Pseudo-dynamic simulation on a district energy system made of coupling technologies. ECOS 2018 - 31st International Conference on Efficiency, Cost, Optimization, Simulation and Environmental Impact of Energy Systems, Guimaraes, Portugal: 2018.
[28] Kennedy J, Eberhart R. Particle swarm optimization. Proceedings of ICNN'95 - International Conference on Neural Networks, vol. 4, 1995, p. 1942–8 vol.4. doi:10.1109/ICNN.1995.488968.
[29] Glover JD, Sarma MS, Overbye T. Power System Analysis & Design, SI Version. Cengage Learning; 2012.
[30] isoplus: Flexible and rigid pipes and pipeline systems: isoplus - isoplus Fernwärmetechnik n.d. http://www.isoplus-pipes.com/ (accessed September 3, 2017).